Mon. Not. R. Astron. Soc. **302,** 807–820 (1999)

The travelling wavelets approach to gravitational instability theory: one-dimensional wavelets

N. Benhamidouche,* B. Torrésani and R. Triay†
Centre de Physique Théorique – CNRS, Luminy Case 907, 13288 Marseille Cedex 9, France

Accepted 1998 October 5. Received 1998 September 8; in original form 1997 December 18

ABSTRACT

We apply the travelling wavelets method to gravitational instability theory for the investigation of large-scale structure formation in cosmology. As the first step of our approach, the method is first applied to the 1D cosmological Euler–Poisson equation system. We test the stability of the linear (evolution) regime in this plane-symmetric case. As a result, our analysis confirms the existence of the linear regime for some configurations of fields describing the evolution of cosmological structures. Moreover, it provides us with estimates for the delay needed for structures of given scale and magnitude to deviate from the linear regime. We also exhibit other configurations for which the linear approximation is not valid *at any time*. In particular, density defaults (i.e. holes) turn out to be highly non-linear structures that dominate the evolution.

Key words: gravitation – instabilities – galaxies: formation – cosmology: theory.

1 INTRODUCTION

The purpose of this paper is to present a new Eulerian approach for studying the large-scale structure formation after decoupling, based on the recently proposed travelling wavelets method (Basdevant et al. 1990).

As usual, we assume a pressureless distribution of matter in an expanding cosmological background. It is well known that the efficiency of gravity in creating structures from fluctuations in a uniform distribution of matter is caused by a (local) instability of the evolutionary equations governing the expansion of the Universe. As the basis of most investigations, the linear theory of perturbations is used as a first step for the understanding the dynamics of such structures, see e.g. Gottlöber (1994), Buchert (1996) and Bouchet (1996). Although the linear regime is assumed to provide an accurate solution for the growth of density fluctuations as long as the density contrast $\delta\rho/\rho < 1$ (Peebles 1993), one may ask whether additional criteria intervene to validate such an approach. In this paper, with the aim of checking the mathematical basis of such an approach, we also investigate the stability of the linear regime. Namely, we integrate the Euler–Poisson equations within an Einstein–de Sitter background by assuming solutions defined by single travelling wavelets. Such an assumption should improve the investigation of the structure formation at large scales, because these functions show vanishing integrals. Indeed, it must be noted that the standard cosmological model requires homogeneity and isotropy of the matter and cosmic velocity distributions, when these constraints are not present in the Euler–Poisson differential equation system.

In order to show clearly the contribution of wavelets in such a problem, and to avoid numerical difficulties and cumbersome mathematics, the present investigation is restricted to its 1D formulation. In this restricted case the general exact solution has been obtained by Zentsova & Chernin and Buchert (1989) in an extended derivation including 3D solutions and other backgrounds. The interpretation of this solution in term of travelling wavelets is discussed in Appendix A4.

The equations governing the evolution of fluctuations are interpreted in term of wavelets with time-dependent parameters, which account for their location, their scale and their amplitude (Section 2). For simplicity, we restrict our investigation to shapes defined by the derivatives of a Gaussian function (Section 3). The solutions can be classified in term of wavelet characteristics (e.g. the linear regime is an artificial evolution where the scales and the positions of fluctuations are constant). With this in mind, the evolution of cosmological structures is investigated under various constraints on their scales and their positions (Section 4). Release from these constraints enables us to investigate the stability problems and additional non-linear effects (Section 5).

Units are chosen so that the speed of the light $c = 1$ and Newton's constant of gravitation $G = 1$. Hence, the time and the mass are measured in units of length ($1\ \mathrm{s} \approx 3 \times 10^{10}$ cm and the unit of mass $1\ \mathrm{g} \approx 7.4 \times 10^{-29}$ cm).

2 WAVELET ANALYSIS OF THE GRAVITATIONAL INSTABILITY

2.1 The 1D gravitational instability

The simplest scenario of large-scale structure formation assumes:

* Present address: Mathematics Department, University of M'Sila BP 254, 28000 M'Sila, Algeria.
† Université de Provence and the European Cosmological Network.

(i) a zero-pressure medium in the Newtonian approximation;

(ii) each structure can be seen as isolated within a given neighbourhood (locality hypothesis);

(iii) the background expands according to the Einstein–de Sitter solution;

(iv) the effects of the space curvature and the cosmological constant are negligible,

although the effect of inhomogeneities on the average expansion may not be negligible (Buchert & Ehlers 1997). Moreover, we assume that the deformation of structures with respect to the Hubble flow can be described by means of a single Cartesian coordinate. Under the above assumptions, we specify the 1D gravitational instability theory (see Appendix A4 for more details) as follows: the energy density of sources (i.e. the mass density field) at comoving distance[1] x and (cosmic) time t is given by

$$\rho(x,t)=\rho_{\rm b}(t)[1+\delta(x,t)]\geq 0, \tag{1}$$

where $\rho_{\rm b}(t)\propto a^{-3}$ describes the background energy density field, $a=a(t)\propto t^{2/3}$ is the (dimensionless) expansion parameter, and $\delta(x,t)\geq -1$ is called the density contrast. As usual the fluctuations are differentiated from the mean in order to investigate their behaviour in term of $\delta(x,t)$ and $u(x,t)$, the *scaled* peculiar velocity fields. The evolution of these fields is governed by the (1D) Euler–Poisson equations, which read (in comoving coordinates)

$$\frac{\partial\delta}{\partial t}+\frac{\partial}{\partial x}[(1+\delta)u]=0, \tag{2}$$

$$\frac{\partial u}{\partial t}+2H\,u+u\frac{\partial u}{\partial x}=-\frac{1}{a^2}\frac{\partial\phi}{\partial x}, \tag{3}$$

$$\frac{1}{a^2}\frac{\partial^2\phi}{\partial x^2}=4\pi\rho_{\rm b}\delta, \tag{4}$$

where $H=\dot{a}/a=2/3t^{-1}$ stands for the Hubble constant and the gravitational potential $\psi=\psi(r,t)$ acts through the function $\phi(x,t)=\psi-1/2\,\ddot{a}x^2$.

By dropping the terms $\partial(\delta u)/\partial x$ and $u\partial u/\partial x$ from equations (2) and (3), one obtains a linear system of differential equations. Its solution reads

$$\delta_0(x,t)=A_1(x)\,t^{2/3}+A_2(x)\,t^{-1}, \tag{5}$$

$$u_0(x,t)=B_1(x)t^{-1/3}+B_2(x)t^{-2}, \tag{6}$$

where the functions $B_{i=1,2}$ are given by

$$B_1(x)=-\frac{2}{3}\int_{-\infty}^{x}A_1(y){\rm d}y,\quad B_2(x)=\int_{-\infty}^{x}A_2(y){\rm d}y, \tag{7}$$

and satisfy $B_i(+\infty)=0$, since the density contrast has a vanishing integral.

The growth of structures in the linear regime is defined by equations (5)–(7). The question of whether such behaviour may be interpreted as an approximation of the true solution or is solely (a solution to) an *ersatz* is discussed in our analysis.

2.2 Travelling wavelets method

The basis of the travelling wavelets method is sketched in Appendix A1. The application of this method to the non-linear differential equation system given in equations (2)–(4) consists of seeking solutions via a non-linear transformation that maps such a system into an ordinary differential equation system, which is easier to solve. The resolution of the latter system is then performed either analytically in the simplest situations or numerically if all the degrees of freedom are taken into account.

In order to use this method it is convenient to write equations (2)–(4) in term of the following function:

$$\omega=\frac{1}{4\pi\rho_{\rm b}a^2}\frac{\partial\phi}{\partial x}. \tag{8}$$

Hence, the density contrast reads $\delta=\partial\omega/\partial x$, and the Euler–Poisson equations (2) and (3) transform into

$$\frac{\partial u}{\partial t}+F_1(\omega,u)=0, \tag{9}$$

$$\frac{\partial}{\partial t}\left(\frac{\partial\omega}{\partial x}\right)+F_2(\omega,u)=0, \tag{10}$$

where the functions $F_{i=1,2}$ are given by

$$F_1(\omega,u)=2H\,u+u\frac{\partial u}{\partial x}+4\pi\rho_{\rm b}\omega, \tag{11}$$

$$F_2(\omega,u)=\frac{\partial}{\partial x}\left[\left(1+\frac{\partial\omega}{\partial x}\right)u\right]. \tag{12}$$

We seek solutions (with wavelet profiles)

$$u(x,t)\approx\psi_1(x,t),\quad \omega(x,t)\approx\psi_2(x,t), \tag{13}$$

where

$$\psi_i(x,t)=c_i\hat{\psi}_i(y_i),\quad y_i=\frac{x-b_i}{a_i} \tag{14}$$

are travelling wavelets, the $\hat{\psi}_i$ define the shape, and the parameters $a_i=a_i(t)$, $b_i=b_i(t)$ and $c_i=c_i(t)$ provide us with the scale, the position and the amplitude. Then the density contrast reads

$$\delta(x,t)\approx\frac{c_2}{a_2}\hat{\psi}_2'(y_2)\geq -1, \tag{15}$$

where $\hat{\psi}_2'={\rm d}\hat{\psi}_2/{\rm d}y_2$.

As the evolution with time of parameters a_i, b_i and c_i specifies the only permitted behaviour for the fields $\psi_{i=1,2}$, it is clear that we obtain approximated solutions. We could have more accuracy by assuming a finite series of travelling wavelets instead of a single one (for each field), but such an approach suffers from the usual shell-crossing problems and has not yet been improved. On the other hand, it is important to note that a single wavelet ensures $\int\delta{\rm d}x=0$ and $\int u{\rm d}x=0$ (as required by the geometry at large scales of a Friedmann universe), while the *ansatz* defined by equations (2)–(4) does not.

Thus the candidate behaviours have to be determined by an error minimization method. Such an optimization problem requires us to define a control of accuracy, which is not a trivial question. Ideally, one would like to control some norm of the difference between the computed solution and the true behaviour. However, with the motivation in mind of investigating the 3D case, the best we can propose to do is to focus on the following (time-dependent) residual functions:

$$\epsilon_1(\psi_2,\psi_1)=\frac{\partial\psi_1}{\partial t}+F_1(\psi_2,\psi_1), \tag{16}$$

$$\epsilon_2(\psi_2,\psi_1)=\frac{\partial}{\partial t}\left(\frac{\partial\psi_2}{\partial x}\right)+F_2(\psi_2,\psi_1). \tag{17}$$

Thus one expects that the smaller the $\mathcal{L}^2(\mathbb{R})$ norm[2] of these terms, the higher the accuracy of solutions.

The optimization method is as follows: the time derivatives of

[1] We recall that the comoving distance is the distance after correction of the expansion; the absolute distance reads $r=a(t)x$, with $a(t)$ the expansion parameter.

[2] The inner product of two functions $f,g\in{}^2(\mathbb{R})$ is given by $\langle f,g\rangle=\int_{\mathbb{R}}f(x)\,g(x){\rm d}x$. Hence, the norm reads in term of the inner product as follows: $\|f\|=\sqrt{\langle f,f\rangle}$.

wavelet parameters are obtained by minimizing (at constant t) the $\mathcal{L}^2(\mathbb{R})$ norm of $\epsilon_{i=1,2}$. Therefore, we obtain six orthogonality equations which read

$$\langle \epsilon_i(\psi_2,\psi_1), \frac{\partial}{\partial \mu_i}\epsilon_i(\psi_2,\psi_1)\rangle = 0, \quad (i=1,2), \tag{18}$$

where $\langle , \rangle$ stands for the $\mathcal{L}^2(\mathbb{R})$ inner product, and the symbol μ denotes the variables $\dot{a}$, $\dot{b}$ and $\dot{c}$ respectively. Hence, we obtain an *ordinary* differential equation system, which can be written as follows:

$$\begin{pmatrix} \mathbf{M}_1 & \mathbf{0}_3 \\ \mathbf{0}_3 & \mathbf{M}_2 \end{pmatrix} \begin{pmatrix} \boldsymbol{X}_1 \\ \boldsymbol{X}_2 \end{pmatrix} = \begin{pmatrix} \boldsymbol{Y}_1 \\ \boldsymbol{Y}_2 \end{pmatrix}, \tag{19}$$

where $\mathbf{0}_3$ denotes the 3×3 null matrix, and the $\mathbf{M}_i$ are 3×3 symmetric matrices defined as follows:

$$\mathbf{M}_1 = \begin{pmatrix} \|\psi_1\|^2 & \langle \psi_1, y_1\psi_1'\rangle & \langle \psi_1, \psi_1'\rangle \\ \cdots & \|y_1\psi_1'\|^2 & \langle y_1\psi_1', \psi_1'\rangle \\ \cdots & \cdots & \|\psi_1'\|^2 \end{pmatrix} \tag{20}$$

$$\mathbf{M}_2 = \frac{1}{a_2^2}\begin{pmatrix} \|\psi_2'\|^2 & \langle \psi_2', \psi_2' + y_2\psi_2''\rangle & \langle \psi_2', \psi_2''\rangle \\ \cdots & \|\psi_2' + y_2\psi_2''\|^2 & \cdots \\ \cdots & \langle \psi_2' + y_2\psi_2'', \psi_2''\rangle & \|\psi_2''\|^2 \end{pmatrix}, \tag{21}$$

where $\psi_i' = \mathrm{d}\psi_i/\mathrm{d}y_i$ and $\psi_i'' = \mathrm{d}^2\psi_i/\mathrm{d}y_i^2$,

$$\boldsymbol{Y}_1 = -\begin{pmatrix} \langle F_1(\psi_2,\psi_1), \psi_1\rangle & (1) \\ \langle F_1(\psi_2,\psi_1), y_1\psi_1'\rangle & (2) \\ \langle F_1(\psi_2,\psi_1), \psi_1'\rangle & \end{pmatrix} \tag{22}$$

$$\boldsymbol{Y}_2 = -\frac{1}{a_2}\begin{pmatrix} \langle F_2(\psi_2,\psi_1), \psi_2'\rangle & (3) \\ \langle F_2(\psi_2,\psi_1), \psi_2' + y_2\psi_2''\rangle & (4) \\ \langle F_2(\psi_2,\psi_1), \psi_2''\rangle & \end{pmatrix} \tag{23}$$

and the unknown variables

$$\boldsymbol{X}_1 = \begin{pmatrix} \dot{c}_1/c_1 \\ -\dot{a}_1/a_1 \\ -\dot{b}_1/a_1 \end{pmatrix}, \quad \boldsymbol{X}_2 = \begin{pmatrix} \dot{c}_2/c_2 \\ -\dot{a}_2/a_2 \\ -\dot{b}_2/a_2 \end{pmatrix} \tag{24}$$

are obtained by inverting equation (19).

Although the evaluation of residues $\|\epsilon_i\|$ at their minimum (δ^*, u^*) provides us with accuracy criteria, dimensionless values are preferred. Such quantities are obtained by normalizing the above values by the linear solution defined in equation (56), which gives

$$\mathrm{Res}_1(t) = \left\|\frac{\partial u_0}{\partial t}\right\|^{-1}\|\epsilon_1\|, \tag{25}$$

$$\mathrm{Res}_2(t) = \left\|\frac{\partial \delta_0}{\partial t}\right\|^{-1}\|\epsilon_2\|. \tag{26}$$

When no formal solution can be found then a numerical scheme is used to solve equations (19)–(24), in both constrained and unconstrained cases (see Sections 4, 5). The time discretization is performed via a standard Adams–Bashforth scheme (Stoer & Bulirsch 1991). Then the matrix $\mathbf{M}$ is inverted by using conjugate gradient methods (Stoer & Bulirsch 1991). Several runs have been made with different time-steps in order to check the accuracy of the scheme. Most of the results presented in this paper have been obtained with a time-step $\delta t = 5\times 10^{-5}\mathrm{Gyr}/h_0$.

2.3 Discussion

The extension of the above formalism to the 3D situation presents no conceptual difficulty. However, it is obvious that the number of degrees of freedom increases, and that special attention has to be paid. Indeed, several 3D generalizations of wavelet analysis may be designed: translations and dilatation may be kept alone, or combined with extra transformations, such as rotations or even more complex transformations. The choice of these new degrees of freedom is far from being innocuous, and it deeply affects the kind of physics that the method will be able to account for.

In this paper, we refrain from considering that level of generality, and postpone the detailed analysis of the 3D problem to a forthcoming publication.

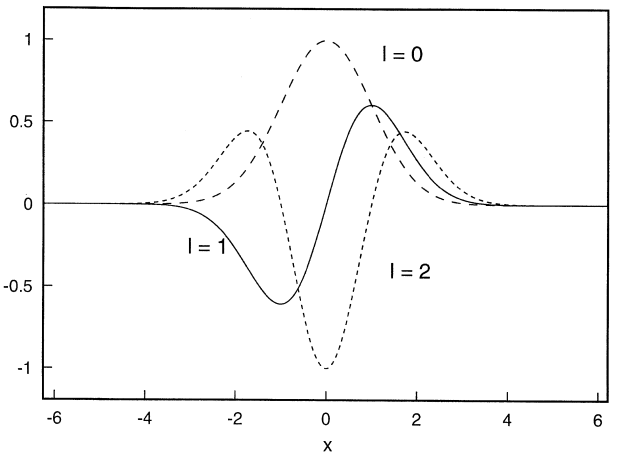

Figure 1. The base wavelets $K_l(x)$, $(l = 0, 1, 2)$.

3 GAUSSIAN-TYPE SHAPE

Part of the analysis we are about to describe does not depend on the particular choice of wavelets. However, for simplicity we have to make a choice, and the derivatives of a Gaussian function

$$K_n(x) = -\frac{\mathrm{d}}{\mathrm{d}x}K_{n-1}(x) \quad (n \geq 1),$$

$$K_0(x) = \mathrm{e}^{-x^2/2}, \tag{27}$$

are used as the base wavelets

$$\hat{\psi}_i = K_{n_i}, \tag{28}$$

(see equation 14), where the integer n stands for the *mode* of the base wavelet. These functions show interesting mathematical properties: they are real functions and well settled in both Fourier and x spaces; their inner products can be written analytically in term of their indices; and they have vanishing moments, which makes the algebra less cumbersome.

The shape of base wavelet K_n is mode-dependent – the larger n, the more oscillating the tails [since the number of roots of equation $K_n(x) = 0$ is equal to n], and the parity of n accounts for symmetries [because $K_n(-x) = (-1)^n K_n(x)$, see Fig. 1]. Namely, we have

(i) a symmetrical shape (even function) if n is even, with either a central bump if $n = 4, 8, \ldots, 4m$, or a central hole if $n = 2, 6, \ldots, 4m-2$; or

(ii) anti-symmetrical shape (odd function) if n is odd, with either a bump to the right-hand side and a hole to the left-hand side if $n = 1, 5, \ldots, 4m-3$, or vice versa if $n = 3, 7, \ldots, 4m-1$;

and the higher the mode the less dominant the central structure (see Fig. 2). It is interesting to note that such an approach provides us with a classification method for *cosmological sub-structures* in term of wavelet characteristics.

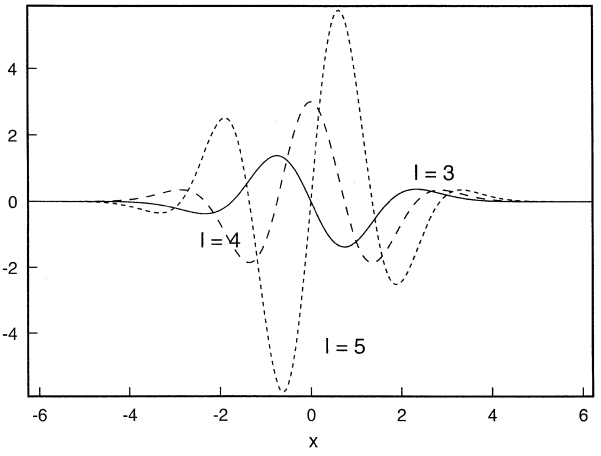

Figure 2. The base wavelets $K_l(x)$, $(l = 3, 4, 5)$.

By assuming that such functions, given in equations (27) and (28), are solutions of equations (9)–(14), the matrix $\mathbf{M}_{i=1,2}$ and the vectors $\boldsymbol{Y}_{i=1,2}$, (see equations 20–23) can be written in term of convolution products of the form

$$J_{m,\ldots,n;p,\ldots,q} = \int_{\mathbb{R}} K_m(y_1)\ldots K_n(y_1)K_p(y_2)\ldots K_q(y_2)\mathrm{d}x \tag{29}$$

where the y_i are given in equation (14), and the subscripts account for modes $n_1 = m\ldots n$ and/or modes $n_2 = p,\ldots,q$. Namely, the J functions read in term of parameters (a_1, b_1) if subscripts are present to the left-hand side of the semicolon and/or in term of parameters (a_2, b_2) if subscripts are present to the right-hand side. The explicit expressions of the J functions are given in Appendix A2.

Hence, the system given in equation (19) transforms as follows: the matrix defined in equation (20) is given by

$$\mathbf{M}_1 = c_1^2\begin{pmatrix} J_{n_1,n_1;} & -\frac{1}{2}J_{n_1,n_1;} & 0 \\ -\frac{1}{2}J_{n_1,n_1;} & \dfrac{4n_1+3}{4}J_{n_1,n_1;} & 0 \\ 0 & 0 & J_{n_1',n_1';} \end{pmatrix} \tag{30}$$

where $n_1' = n_1 + 1$; the matrix defined in equation (21) is given by

$$\mathbf{M}_2 = \frac{c_2^2}{a_2^2}\begin{pmatrix} J_{;n_2',n_2'} & \frac{1}{2}J_{;n_2',n_2'} & 0 \\ \frac{1}{2}J_{;n_2',n_2'} & \dfrac{4n_2+7}{4}J_{;n_2',n_2'} & 0 \\ 0 & 0 & J_{;n_2'',n_2''} \end{pmatrix} \tag{31}$$

where $n_2' = n_2 + 1$ and $n_2'' = n_2 + 2$; and finally the vector defined in equations (22) and (23) is given by

$$\boldsymbol{Y}_1 = \begin{pmatrix} \begin{bmatrix} \dfrac{c_1^3}{a_1}J_{n_1,n_1',n_1;} - \dfrac{4}{3}t^{-1}c_1^2a_1J_{n_1,n_1;} \\ -\frac{2}{3}t^{-2}c_1c_2a_1J_{n_1;n_2} \end{bmatrix} \\ \begin{bmatrix} -\dfrac{c_1^3}{a_1}\left(J_{n_1,n_1',n_1+2;} + n_1'J_{n_1,n_1',n_1;}\right) \\ +\frac{4}{6}t^{-1}c_1^2a_1J_{n_1,n_1;} \\ -\frac{2}{3}t^{-2}c_1a_1c_2\left(J_{n_1+2;n_2} + n_1'J_{n_1;n_2}\right) \end{bmatrix} \\ -\dfrac{{c_1}^3}{a_1}J_{n_1,n_1',n_1';} + \dfrac{2}{3}t^{-2}c_1a_1c_2J_{n_1';n_2} \end{pmatrix}, \tag{32}$$

$$\boldsymbol{Y}_2 = \frac{c_1c_2}{a_2^2}\begin{pmatrix} -J_{n_1';n_2'} - \dfrac{c_2}{a_2}J_{n_1;n_2',n_2''} \\ \begin{bmatrix} J_{n_1';n_2+3} + n_2'J_{n_1';n_2'} \\ +\dfrac{c_2}{a_2}\left(J_{n_1;n_2',n_2+4} + n_2'J_{n_1;n_2',n_2''}\right) \end{bmatrix} \\ J_{n_1';n_2''} + \frac{c_2}{a_2}J_{n_1;n_2',n_2+3} \end{pmatrix}. \tag{33}$$

3.1 Analysis of solutions

It is convenient to define a *state* (or configuration) by the pair of integers (n_1, n_2), in which the cosmological structure evolves from given boundary conditions $a_i = a_i(t)$, $b_i = b_i(t)$ and $c_i = c_i(t)$ at date $t = t_0$. Since we deal with approximations, the true solution may, however, deviate from it with time. Then the analysis of residuals is the only way to validate candidate behaviour. The calculations show that in general one has $\mathrm{Res}_2 \gg \mathrm{Res}_1$, which suggests that the quality criterion can be based solely on the residual Res_2.

Moreover, we easily understand that physical interpretations of this behaviour are also useful in order to prevent our analysis from containing artefacts. Such an analysis can be performed by taking into account the profiles of fields. The *central part* of a field exhibits the following shape:

(i) the density contrast is symmetrical if n_2 is odd, which defines either a density *excess* if $n_2 = 3, 7, \ldots 4m - 1$, or a density *default* if $n_2 = 1, 5, \ldots 4m - 3$, and anti-symmetrical if n_2 is even, which defines a *gutter*-like structure (neighbouring excess and default density);

(ii) the velocity field indicates whether the structure is *expanding* $(n_1 = 1, 5, \ldots, 4m - 3)$, *collapsing* $(n_1 = 3, 7, \ldots, 4m - 1)$ or (simply) *shifting*.

It is important to emphasize that these velocities account for local displacements. On the other hand, variations of the position parameters b_i correspond to large-scale velocity fields, e.g. Lauer & Postman effect-like.

Thus identical wavelet parameters for both fields account for a cluster composed of a main central structure surrounded by neighbouring ones, which evolves regularly (simpler structure for the lower the modes) from 'soft boundary conditions', when 'complex evolutions' may be described by states such that the modes $n_1 \neq n_2$. On the other hand, we expect that very different wavelet parameters $a_1 \neq a_2$ or $b_1 \neq b_2$ produce less reliable solutions (in particular for the position parameter). Such situations are investigated mainly to check the stability of solutions.

4 STRUCTURES AT FIXED POSITIONS AND CONSTANT SCALES

The constraints $\dot{a}_{i=1,2} = 0$ and $\dot{b}_{i=1,2} = 0$, with equations (9)–(10), define cosmological structures which evolve at fixed position and constant scale. Their evolution depends on the following dimensionless quantities:

$$w = a_1/a_2, \qquad v = (b_1 - b_2)/a_2, \tag{34}$$

and satisfies equation (19), which reads

$$\frac{\dot{c}_1}{a_1} = \lambda_2\left(\frac{c_1}{a_1}\right)^2 - \frac{4}{3}\frac{c_1}{a_1}t^{-1} - \frac{2}{3}\frac{1}{w}\lambda_1\frac{c_2}{a_2}t^{-2}, \tag{35}$$

$$\frac{\dot{c}_2}{a_2} = w\left(\lambda_3\frac{c_2}{a_2} - \lambda_4\frac{c_1}{a_1}\right), \tag{36}$$

where the λ functions account for the ratios of J terms,

$$\lambda_1(n_1,n_2,w,v)=\frac{J_{n_1;n_2}}{J_{n_1,n_1;}}, \tag{37}$$

$$\lambda_2(n_1)=\frac{J_{n_1,n_1+1,n_1;}}{J_{n_1,n_1;}}, \tag{38}$$

$$\lambda_3(n_1,n_2,w,v)=\frac{J_{n_1;n_2+1,n_2+2}}{J_{;n_2+1,n_2+1}}, \tag{39}$$

$$\lambda_4(n_1,n_2,w,v)=\lambda_1(n_2,n_1,1/w,-v/w). \tag{40}$$

It is interesting to note in equation (36) that the evolution of the density contrast depends strongly on the velocity field, although equation (35) shows that the evolution of the latter decouples with time. Such a feature is characteristic of gravitational instability behaviour. A rough analysis of the coupling shows that the contribution of the first right-hand term of equation (35) gives a virtual behaviour $c_1 \approx a_1 c_1(t_0)\left[a_1-\lambda_2(n_1)c_1(t_0)(t-t_0)\right]^{-1}$. Thus the larger the magnitude of the velocity field, the larger λ_2, even though the effect of the other two terms works against the evolution toward such an asymptotic state, since c_2 increases with c_1, see equation (36).

The equations system given in equations (35) and (36) depends on the symmetry properties of the J terms given in equations (37)–(40), which accounts for the correlation of modes $n_{i=1,2}$. Hence, we propose an investigation with regard to the parity of wavelet modes, and we group (a posteriori) the solutions into three classes, in which (i) both modes are even, (ii) both are odd, or (iii) they show different evenness.

In general, we seek a *numerical solution* obtained by computer methods, although the λ functions vanish for some combination of modes. Hence, equations (35) and (36) may transform into classes of differential equation systems with a known analytical solution. Such a situation can happen when the fields show the same positions, and does not depend on their scale parameters – see equations (37) and (39) and Appendix A2. With this in mind, the analysis is performed by taking into account whether $a_1=a_2$ and/or $b_1=b_2$, and we use the following notation:

$$\begin{aligned}&\alpha=a_{i=1,2} \qquad \text{if } a_1=a_2,\\ &y=(x-b_i)/\alpha \quad \text{if } b_1=b_2.\end{aligned} \tag{41}$$

The case $w\ll 1$ accounts for local displacements involving a small part of the central structure, while $w\gg 1$ accounts for structures embedded in velocity fields.

4.1 States with even modes

If the modes are even, $n_{i=1,2}\geq 2$, then the central regions of related structures are shifting gutters (a density excess near to a density default, which shows a local displacement).

4.1.1 The case ($a_1=a_2$, $b_1=b_2$)

If $b_1=b_2$ then $\lambda_2=\lambda_3=0$ (since the terms $J_{n_1;n_2+1,n_2+2}$ and $J_{n_1,n_1+1,n_1;}$ vanish), and equations (35) and (36) give scale-independent equations, which can be combined to provide us with

$$\frac{\partial^2 c_2}{\partial t^2}+\frac{4}{3t}\frac{\partial c_2}{\partial t}=\frac{2}{3t^2}\tau_0(n_2,n_1)c_2, \tag{42}$$

[3] We recall that the double factorial symbol has the following meaning:

$$n!!=n(n-2)(n-4)\ldots$$

$$=\begin{cases}2^{n/2}(n/2)! & \text{if } n \text{ is even},\\ n!/[2^{(n-1)/2}((n-1)/2)!] & \text{if } n \text{ is odd}.\end{cases}$$

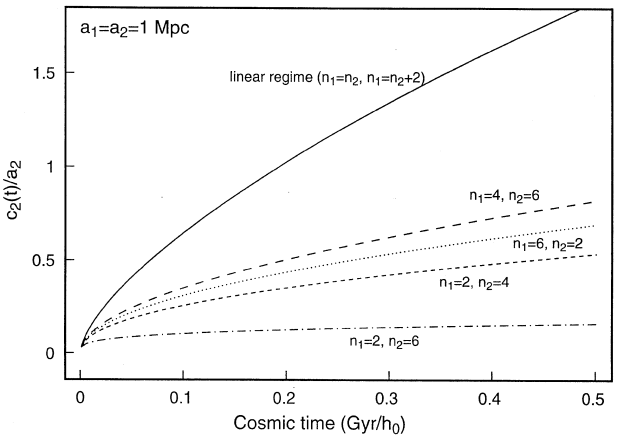

Figure 3. Evolution of the magnitude of density contrast $\delta=c_2/a_2$ for even modes $(n_1,n_2=2,4,6)$; the *linear regime* is given by the constraint $(n_1-n_2=0,2)$. The structure is defined by $a_1=a_2=1$ Mpc and $b_1=b_2$.

where the function[3]

$$\tau_0(m,n)=\frac{(m+n+1)!!(m+n-1)!!}{(2m+1)!!(2n-1)!!} \tag{43}$$

takes discrete values within $0<\tau_0\leq 1$ (see Appendix A3). Hence, we obtain a set of power-law solutions defined by

$$c_1(t)=-\frac{J_{n_2,n_2;}}{J_{n_1;n_2}}\left(l_{\rm u}k_{\rm u}t^{l_{\rm u}-1}+l_{\rm d}k_{\rm d}t^{l_{\rm d}-1}\right), \tag{44}$$

$$c_2(t)=k_{\rm u}t^{l_{\rm u}}+k_{\rm d}t^{l_{\rm d}}, \tag{45}$$

where

$$l_{\rm u}=\frac{-1+\sqrt{1+24\tau_0(n_2,n_1)}}{6}, \tag{46}$$

$$l_{\rm d}=\frac{-1-\sqrt{1+24\tau_0(n_2,n_1)}}{6}; \tag{47}$$

the k_r are integration constants related to a growing mode ($r=$ u) and a decaying mode ($r=$ d), with

$$0<l_{\rm u}\leq\frac{2}{3},\quad -1\leq l_{\rm d}<-\frac{1}{3}, \tag{48}$$

see equation (A16). If the decaying mode is neglected then the (normalized) residuals are given by

$$\begin{aligned}{\rm Res}_1(t)^2=&\frac{\|\frac{2\lambda_1}{3}K_{n_2}-l(l+\frac{1}{3})K_{n_1}\|^2}{l^2(l-1)^2\|K_{n_1}\|^2}\\ &+\frac{k^2l^2}{\alpha^2(l-1)}\frac{\|K_{n_1}K_{n_1+1}\|^2}{\|K_{n_1}\|^2}t^{2l},\end{aligned} \tag{49}$$

$$\begin{aligned}{\rm Res}_2(t)^2=&\frac{\|\lambda_1K_{n_2+1}-K_{n_1+1}\|^2}{\|\lambda_1K_{n_2+1}\|^2}\\ &+\frac{k^2}{\alpha^2}\frac{\|\left(K_{n_1}K_{n_2+1}\right)'\|^2}{\|K_{n_2+1}\|^2}t^{2l},\end{aligned} \tag{50}$$

(see equations 25 and 26), where $l=l_{\rm u}$ and $k=k_{\rm u}$. In both cases, the first term on the right-hand side is a bias due to the method, while the second one is due to an error which increases with time and depends on the scale parameter α.

It is interesting to mention that this set of solutions can be arranged in order of increasing value of τ_0 within the bounded domain $0<\tau_0\leq 1$ (see equations 43 and A16). The larger the value, the faster the evolution of structures with time. The highest value $\tau_0(n_2,n_1)=1$ defines a behaviour which dominates the evolution (see Fig. 3). The related modes are such that $n_1-n_2=0,2$, and the fields read as follows:

(i) if $n_1 = n_2 = 2n$ then

$$\delta(x,t) \approx \frac{k_u}{\alpha} K_{2n+1}(y) t^{2/3} + \frac{k_d}{\alpha} K_{2n+1}(y) t^{-1} \quad (51)$$

$$u(x,t) \approx -\frac{2}{3} k_u K_{2n}(y) t^{-1/3} + k_d K_{2n}(y) t^{-2}; \quad (52)$$

(ii) if $n_1 = n_2 + 2 = 2n$ then

$$\delta(x,t) \approx \frac{k_u}{\alpha} K_{2n-1}(y) t^{2/3} + \frac{k_d}{\alpha} K_{2n-1}(y) t^{-1} \quad (53)$$

$$u(x,t) \approx \frac{J_{2n-2,2n-2;}}{J_{2n;2n-2}} \left[-\frac{2}{3} k_u K_{2n}(y) t^{-\frac{1}{3}} + k_d K_{2n}(y) t^{-2} \right]. \quad (54)$$

These solutions identify the (usual) *linear regime* (see equations 5 and 6). However, it must be noted that, although they show the same temporal behaviour, the velocity field amplitude of the $(n_1 = n_2 + 2)$ solutions does not satisfy equation (7). It is important to remind the reader that this constraint is not required for solutions of the equations system given by equations (2)–(4) but rather for its linear ersatz. The accuracies of these solutions are given as follows:

(i) if $n_1 = n_2 = 2n$ then

$$\mathrm{Res}_1(t) = 2\frac{k}{\alpha} \frac{\|K_{2n} K_{2n+1}\|}{\|K_{2n}\|} t^l, \quad (55)$$

$$\mathrm{Res}_2(t) = \frac{k}{\alpha} \frac{\| \left(K_{2n} K_{2n+1}\right)' \|}{\|K_{2n+1}\|} t^l; \quad (56)$$

(ii) if $n_1 = n_2 + 2 = 2n + 2$ then

$$\mathrm{Res}_1(t)^2 = 9 \frac{||K_{2n+2} - \lambda_1 K_{2n}||^2}{||K_{2n+2}||^2} + 4\frac{k^2}{\alpha^2} \frac{\|K_{2n+2} K_{2n+3}\|^2}{\|K_{2n+2}\|^2} t^{2l}, \quad (57)$$

$$\mathrm{Res}_2(t)^2 = \frac{\|K_{2n+3} - \lambda_1 K_{2n+1}\|^2}{\|\lambda_1 K_{2n+1}\|^2} + \frac{k^2}{\alpha^2} \frac{\| \left(K_{2n+2} K_{2n+1}\right)' \|^2}{\|K_{2n+1}\|^2} t^{2l}. \quad (58)$$

Hence, we see that the $(n_1 = n_2)$ solution is more reliable than the $(n_1 = n_2 + 2)$ one because the systematic bias vanishes (see Fig. 4), and the larger the discrepancy between the modes, the higher the residual (e.g. see the curves $n_1 = n_2 + 2 = 4, 6$). These results will be confirmed in the next section when discussing modes with non-constant position and scale.

Finally, it turns out that the larger the discrepancy between the modes $n_{i=1,2}$, the slower the growth of fluctuations (see Fig. 3), and the higher the residues Res_2 (see Fig. 4). This is a consequence of equation (46) and the fact that $\tau_0(2m, 2n)$ (and thus l_u) are decreasing functions of $|m - n|$ (see Appendix A3).

Let us emphasize that by choosing a threshold $\overline{\mathrm{Res}_i}$ upon these residues ($\mathrm{Res}_i(t) < \overline{\mathrm{Res}_i}$) we obtain a sensible definition for linearity criteria (and thus an exit date from such a regime). The above equations show clearly that the larger the scale of a cosmological structure, the longer it lies in the linear regime, but also that the exit criteria depend on the magnitude of the density contrast,[4] and on the wavelet modes.

4.1.2 *The cases $(a_1 \neq a_2)$ and/or $(b_1 \neq b_2)$*

Let us investigate the cases where the scales and/or the positions are unmatched. For the $(a_1 \neq a_2, b_1 = b_2)$ case, the solutions read as in equations (44) and (45), but where $\tau_0(n_2, n_1)$ is substituted by

$$\tau_1(m,n,w) = \tau_0(m,n) \frac{2^{m+n+2} w^{2n+2}}{(1+w^2)^{m+n+2}}, \quad (59)$$

which satisfies $0 \leq \tau_1 \leq 1$. The analysis of behaviour shows that the linear regime ($n_1 - n_2 = 0, 2$, $w = 1$) still dominates (see Fig. 5). Moreover, other numerical results (not presented here) show that the more different the scales, the less reliable the solution. It is interesting to note that the function $\tau_1 \to 0$ when $w \to 0$ or $w \to \infty$, which makes $l_u \to 0$ and $l_d \to -1/3$. In other words, if the scales are very different then the velocity field vanishes and the density contrast converges toward a constant structure.

Similar results are obtained in the case $(a_1 = a_2,\ b_1 \neq b_2)$. Compared with the solutions given in equations (44) and (45), the behaviour of the density contrast accounts for the correlation term related to $\lambda_3 \neq 0$. The analysis of solutions shows that again the larger the shift v between the fields, the slower the growth of the density contrast (see Fig. 6) and the higher the residual Res_2.

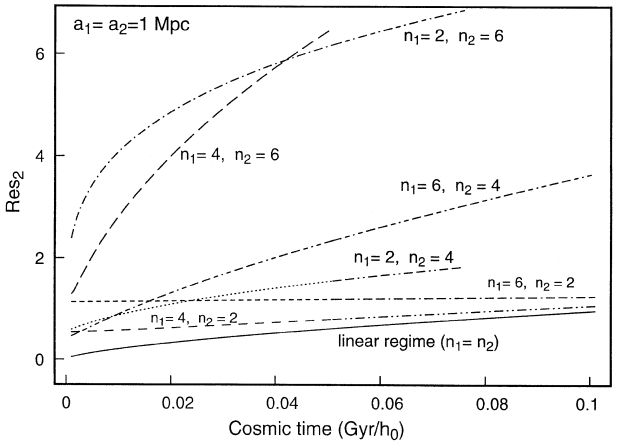

Figure 4. The residual Res_2 for even modes $(n_1, n_2 = 2, 4, 6)$; the *linear regime* is given by the constraint $(n_1 = n_2)$. The structure is defined by $a_1 = a_2 = 1$ Mpc and $b_1 = b_2$.

4.2 States with odd modes

If the state is defined by odd modes $n_{i=1,2} \geq 1$ then none of the J terms vanishes, and equations (35) and (36) define a non linear system that we solve by means of computer methods.

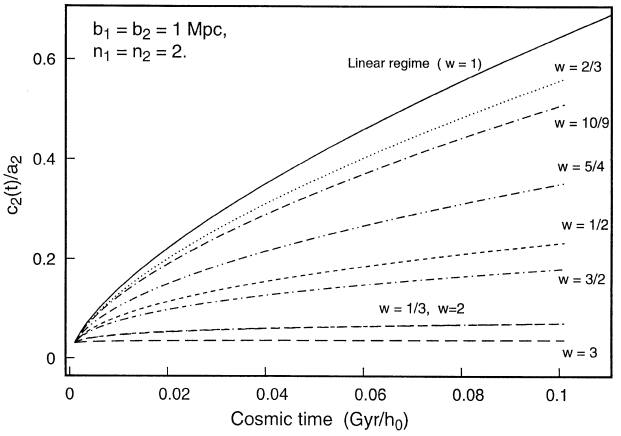

Figure 5. Magnitude of density contrast as a function of $w = a_1/a_2$ for with $(n_1 = n_2 = 2)$ solution, with scale $a_2 = 1$ Mpc and $b_1 = b_2$.

[4] Let us recall that density contrast $\delta(t) \propto \frac{k_u}{\alpha} t^l$ – see equations (51) and (53).

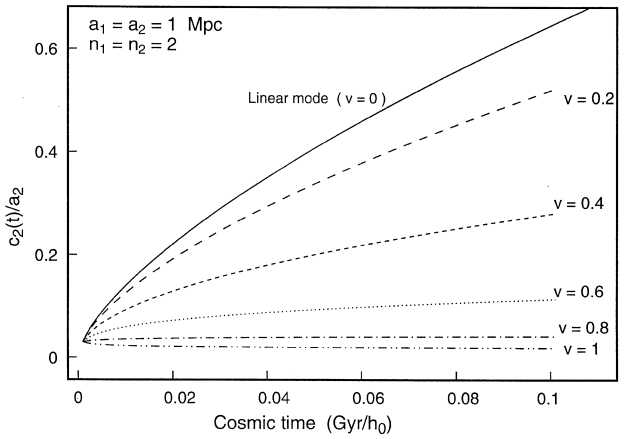

Figure 6. Magnitude of the density contrast for different values of $v = (b_1 - b_2)/a_2$ for the $(n_1 = n_2 = 2)$ solution, with scale $a_1 = a_2 = 1$Mpc.

4.2.1 *The case* $(a_1 = a_2,\ b_1 = b_2)$

The regular structures $(n_1 = n_2)$ are either collapsing density excesses $(n_i = 4m - 1)$, with growth slower than the linear regime, or expanding density defaults $(n_i = 4m - 3)$, with growth faster than the linear regime (see Fig. 7). Moreover, the higher the mode the faster the growth for density defaults and the slower the growth of density excess. The analysis of residuals shows that the $(n_1 = n_2 = 1)$ state is even more accurate than the linear regime (see Fig. 8). Such behaviour clearly indicates that the usual linearity criteria $(\delta < 1)$ fail if the initial conditions are defined by odd modes.

4.2.2 *The cases* $(a_1 \neq a_2)$ *and/or* $(b_1 \neq b_2)$

As before, let us start with the case where only the scales are unmatched. As may be seen from Fig. 9, the $w = 1$ solution dominates, and the more different the scales, the slower the growth of density fluctuations (see Fig. 9), and the less reliable the solution (up to a given date).

As expected, when the positions do not match, the larger the shift v between the fields, the slower the growth of the density contrast, and the $v = 1$ solution dominates (see Fig. 10).

Finally, the analysis of solutions shows that the dominant behaviour is defined such that the scale and the position of the density contrast coincide with those of the velocity field.

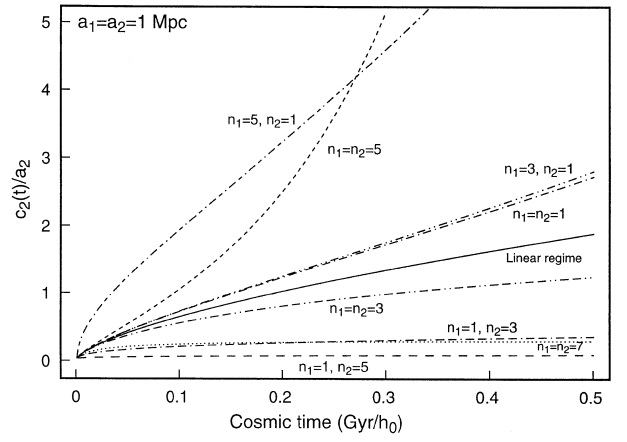

Figure 7. Magnitude of the density contrast for odd modes $(n_i = 1, 3, 5, 7)$, with scale $a_1 = a_2 = 1$Mpc and position $b_1 = b_2$. The linear regime, defined by the state $(n_1 = n_2 = 2)$, is given by the continuous line.

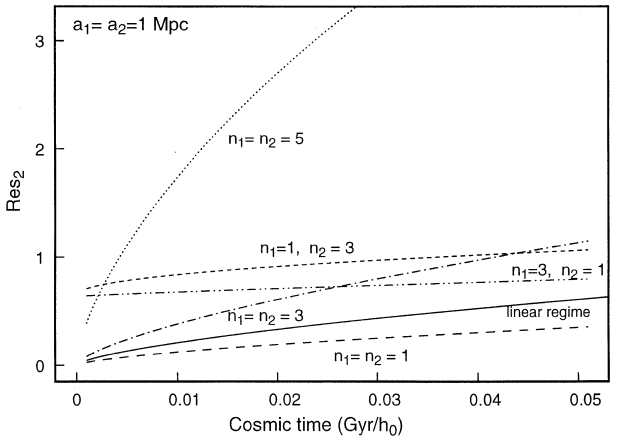

Figure 8. Residual Res_2 for the $(n_i = 1, 3, 5, 7)$ solutions, with scale $a_1 = a_2 = 1$Mpc and position $b_1 = b_2$. The linear regime, defined by the state $(n_1 = n_2 = 2)$, is given by the continuous line.

4.3 States with different evenness modes

According to the definitions given above, we identify related structures, which are classified as follows.

(i) If $(n_1 = 2q, n_2 = 2p + 1)$ then they show a shifting central feature, which is either an excess or default of density,

(ii) if $(n_1 = 2q + 1, n_2 = 2p)$ then the central component looks like a gutter which either expands or collapses.

As we shall see, compared with previous behaviour, these modes show peculiar evolution toward stable configurations (vanishing peculiar velocities providing us with static density contrasts). In this paper, we only describe the cases where scales and positions are matched, and we refer to Benhamidouche (1995) for a discussion of other configurations. We have two situations:

(i) If $(n_1 = 2q, n_2 = 2p + 1)$ then $\lambda_1 = \lambda_3 = 0$, and the terms $J_{n_1;n_2}$, $J_{n_1+1;n_2+1}$, $J_{n_1;n_2+1,n_2+2}$ and $J_{n_1,n_1+1,n_1;}$ vanish. The solution reads

$$c_1(t) = k_1 t^{-\frac{4}{3}}, \tag{60}$$

$$c_2(t) = k_2, \tag{61}$$

where the $k_{i=1,2}$ are constants. Hence, the density contrast and the

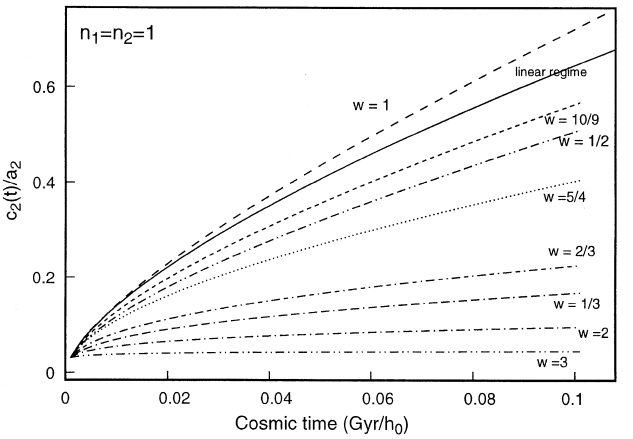

Figure 9. Magnitude of the density contrast versus $w = a_1/a_2$ for the $(n_1 = n_2 = 1)$ solution, with scale $a_2 = 1$Mpc and position $b_1 = b_2$.

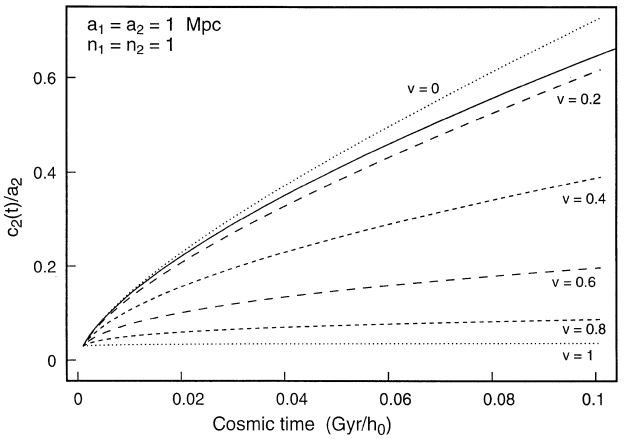

Figure 10. Magnitude of the density contrast versus $v = (b_1 - b_2)/a_2$ for the $(n_1 = n_2 = 1)$ solution, with scale $a_1 = a_2 = 1$ Mpc.

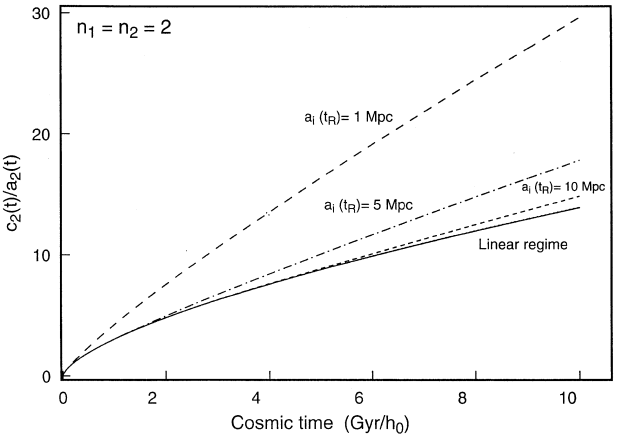

Figure 11. Evolution of the magnitude of density contrast $\delta = c_2/a2$ for even modes $(n_1 = n_2 = 2)$, for several scales: $a_1 = a_2 = 1, 5$ and 10 Mpc and $b_1 = b_2$.

velocity fields are given by

$$\delta(x,t) \approx \frac{k_2}{\alpha} K_{2p+2}(y), \tag{62}$$

$$u(x,t) \approx k_1 K_{2q}(y) t^{-4/3}. \tag{63}$$

Such behaviour describes stable structures: constant contrast and velocity fields varying with time, asymptotically vanishing. It turns out that the residual Res_2 becomes useless because $\partial\delta/\partial t = 0$. Therefore, we are forced to limit ourselves to the other residual Res_1 to investigate the accuracy of these solutions:

$$\mathrm{Res}_1(t) = \frac{1}{\|k_1 K_{2q}\|} \| \frac{k_1^2}{\alpha} K_{2q} K_{2q+1} t^{-1/3} + \frac{2}{3} k_2 K_{2p+1} t^{1/3} \|. \tag{64}$$

This term does not go to zero as t grows, which suggests that such behaviour is either poorly determined by the wavelets method or is an artefact.

(ii) If $(n_1 = 2q+1, n_2 = 2p)$ then the terms $J_{n_1;n_2}$ and $J_{n_1;n_2}$ vanish (i.e., $\lambda_1 = \lambda_3 = 0$), and Eq. (27) transforms into a (scale-independent) Bernoulli-type equation. The solution may be obtained explicitly and reads

$$c_1(t) = a_1 \left(3\lambda_2 t + k_1 a_1 t^{4/3}\right)^{-1}, \tag{65}$$

$$c_2(t) = k_2 \left[t^{1/3} \left(1 + \frac{1}{3} k_1 \frac{a_1}{\lambda_2} t^{1/3} \right)^{-1} \right]^{(a_1\lambda_3)/(a_2^2\lambda_2)}, \tag{66}$$

where the λ_i are given in equations (38) and (39) with $w = 1$ and $v = 0$, and the $k_{i=1,2}$ are constants. By noting that $c_1 \sim k_1^{-1} t^{-4/3}$ and $c_2 \approx k_2 (3\lambda_2/k_1\alpha)^{\lambda_3/\alpha\lambda_2}$ when $t \to \infty$, we see that this behaviour is asymptotically equivalent to the previous one $(n_1 = 2q,\ n_2 = 2p+1)$, with similar residuals, and thus the analysis of this solution provides us with equivalent results.

Although the relevance of these types of behaviour may be rather questionable or poorly determined, they are less stringent than the stable clustering hypothesis (Jain 1997).

5 UNCONSTRAINED BEHAVIOUR

We now turn to the general case, in which the structures show characteristics of scale and position which are time-dependent functions. The goal of this section is twofold, to investigate

(i) the stability of the linear regime, and

(ii) the behaviour of 'non-linear' regimes as exhibited in the previous sections.

5.1 States with even modes

Let us remember that, at constant scale and position, the states defined by even modes (i.e. the case where n_1 and n_2 are even numbers) provide us with behaviour compatible with the linear regime. We understand that the structure exits from the linear regime when the variations of the position and scale parameters become significant. We now solve by numerical methods the system of non-linear ordinary differential equations given in equation (19). An example of the results that we obtain is given in Fig. 11, which shows the amplitude c_2 of the density contrast as a function of time, for several structures with different initial scales. As expected, the time evolution of the amplitude deviates from the linear regime after a given period of time. It turns out that the length at which the deviation becomes significant is a decreasing function of the initial scale. In other words, the structures at small scales leave the linear regime earlier. Fig. 12 shows the time evolution of the normalized amplitude

$$\tilde{c}_2(t) = t^{-2/3} c_2(t) \tag{67}$$

and the scale a_2, for an initial scale $a_1 = a_2 = 1$ Mpc at $t = t_0$. It is clear that the non-linearity effect can be interpreted as an amplification of the structure (the amplitude increases) when the scale decreases. This suggests the use of numerical simulations to

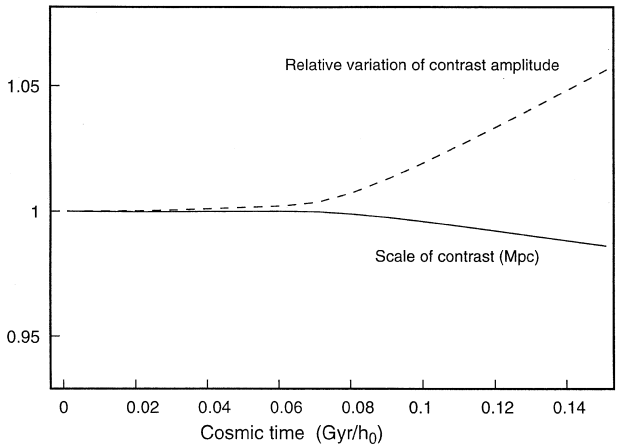

Figure 12. Evolution of the scale and the normalized magnitude of density contrast $\delta = c_2/a2$ for even modes $(n_1 = n_2 = 2)$. The structure is defined by $a_1(t_0) = a_2(t_0) = 1$ Mpc and $b_1 = b_2$.

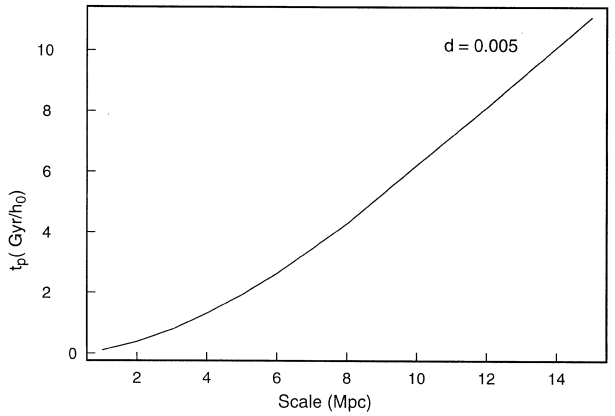

Figure 13. Linearity time for a structure as a function of the initial scale.

obtain an estimate for the time needed for a structure to exit from the linear regime. This may be done as follows. Let d be a fixed *discrepancy* limit. We say that the structure is non-linear at the discrepancy level d if $\tilde{c}_2 \geq d$. For given structure and discrepancy level d, we shall denote by t^* the *linearity time*, i.e. the time needed for the structure to 'become non-linear". More precisely, t^* is defined as the value of t such that

$$\tilde{c}_2(t) \geq d\,, \quad \forall t \geq t^*. \tag{68}$$

As stressed before, t^* is an increasing function of the initial scale (large structures are linear for a longer time). An example of variation of the linearity time t^* as a function of the initial scale $a_2(t_0)$ is given in Fig. 13; the discrepancy level is $d = 0.005$ (other values lead to similar behaviour).

5.2 States with odd modes

Let us remember that, at constant scale and position, the states defined by odd modes have already led to 'non-linear" behaviour. As may be seen from Fig. 14 the growth of the amplitude of the structure becomes much faster in this new situation, showing that such configurations are highly non-linear. This fact is confirmed by the study of the time evolution of the scales of the velocity a_1 and density contrast a_2. It is clearly seen in Fig. 15 that the scale decreases as a function of time, which shows that the corresponding structures tend to get smaller and smaller as time increases, while the amplitude of contrast grows.

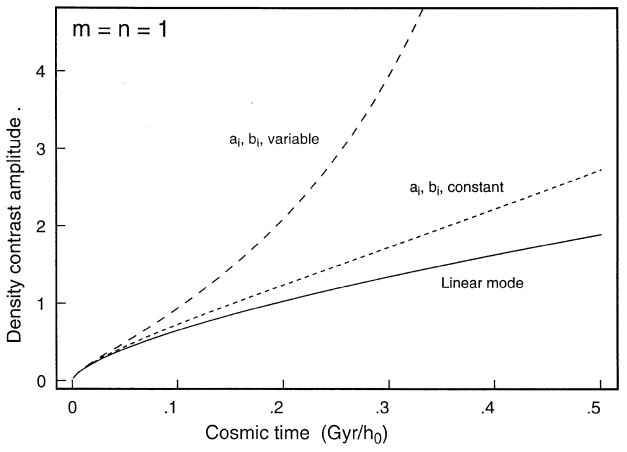

Figure 14. Amplitude of the density contrast as a function of time in three situations: linear regime, constrained modes unconstrained modes.

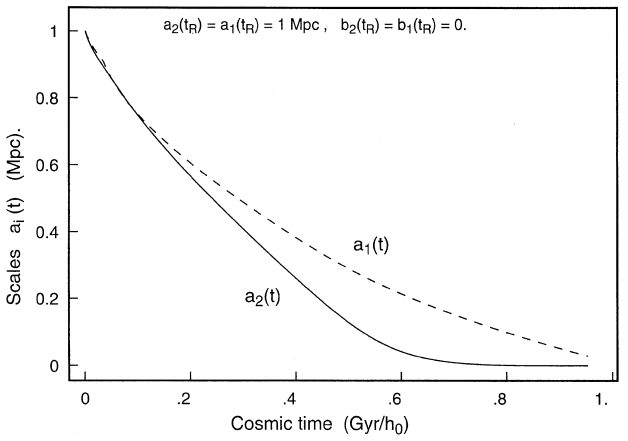

Figure 15. Evolution of the scales of the density contrast and peculiar velocity as functions of time in the unconstrained situation.

5.3 States with different evenness modes

We have also investigated the other modes, which appeared to be stable in the constrained situation. In the unconstrained case, such modes exhibit similar behaviour: they have a short evolution till they become stable. Again, this case does not seem relevant. Again, we refer the reader to Benhamidouche (1995) for a more complete discussion of those cases.

6 CONCLUSION

The formation and evolution of large-scale structures in a 1D space are investigated by means of the travelling wavelets method with the goal of extending this programme to the 3D case. We derive the temporal evolution of the scale, the position and the amplitude of structures, which are assumed to evolve within a shape given by derivatives of a Gaussian function. The order of the derivative (the mode) characterizes the shape of the wavelet: the larger mode, the more oscillating the tails. Thus this behaviour belongs to an approximation space and is defined in terms of a couple of integers which give the modes of wavelets, one for the density contrast and the other for the velocity fields. The analysis of residuals and the use of a threshold ensure the likelihood of candidate solutions and provide us with sensible criteria to define a regime within a given accuracy.

Our analysis confirms the existence of a *linear regime* , understood as a solution of the complete set of Euler–Poisson equation systems. However, it turns out that the usual criterion $\delta < 1$ is not sufficient to ensure such a regime for any structure. In particular, it becomes obvious that large-scale structures show a linear regime for a longer time than ones at smaller scales. An exit criterion is derived which involves the complexity and the scale of the structure, in addition to its amplitude. Hence, estimates for the time spent by a structure of a given size in the linear regime can be calculated. Moreover, it turns out that the growth of structures exhibits a high sensitivity to initial conditions. In particular, there are structures that do not evolve in the linear regime.

The expanding density defaults (odd modes) are actually the structures that dominate, the faster the growth the more complex the structure (i.e. the higher the mode). The shifting gutters (even modes) are structures that evolve slower. They form a one-bounded parameter family of solutions, in which the linear regime belongs to the boundary and dominates the others. On the other hand, the

collapsing density excesses (odd modes) show much slower evolution, the slower the growth the more complex the structure.

Extrapolating this result to 3D cosmology would suggest that the expansion of voids is the clue to the understanding of the problem of large-scale structure formation. A detailed treatment of this more realistic situation is in progress, and a version which takes into account different background cosmologies is envisaged.

ACKNOWLEDGMENTS

We thank B. Jones, S. Rauzy and J.M. Souriau for fruitful discussions, and V. Perrier for her help in developing travelling wavelets numerical algorithms. We thank T. Buchert for valuable comments and suggestions.

REFERENCES

Basdevant C., Holschneider M., Perrier V. 1990, C. R. Acad. Sci. Paris, 310, 647
Benhamidouche N. 1995, PhD thesis, CPT Marseilles
Bouchet F. R., 1996, in Bonometto S., Primack J., Prvenzale A., eds, Proc. Int. School Phys. Enrico Fermi, Course CXXXII, Dark Matter in the Universe. IOP Press, Amsterdam
Buchert T., 1989, A&A, 223, 9
Buchert T., 1996, in Bonometto S., Primack J., Provenzale A., eds, Proc. Int. School Phys. Enrico Fermi, Course CXXXII: Dark Matter in the Universe. IOP Press,Amsterdam, p. 543
Buchert T., Ehlers J., 1997, A&A, 320, 1
Doroshkevich A. G., Shandarin S. F., 1973, Afz, 9, 549
Doroshkevich A. G., Ryaben'kii V. S., Shandarin S. F., 1973, AFz, 9, 257
Gottlöber S., 1994, in Novello M., ed., Cosmology and Gravitation. Editions Frontières
Jain B., 1997, MNRAS, 287,687
Lauer T. R., Postman M., 1994, ApJ, 425, 418
Peebles P. J. E., 1993, Principles of Physical Cosmology. Princeton Univ. Press, Princeton NJ
Shandarin S. F., Zeldovich Ya.B., 1984, Phys. Rev. Lett., 52, 1488
Shandarin S. F., Zeldovich Ya.B., 1989, Rev. Mod. Phys., 61, 185
Stoer J., Bulirsch R., 1991, Texts in Applied Mathematics 12, Introduction to Numerical Analysis. Springer Verlag, p. 456
Susperregi M., Buchert T., 1997, A&A, 323, 295
Zel'dovich Ya.B., 1970a, A&A, 5, 84
Zel'dovich Ya.B., 1970b, Afz, 6, 319
Zentsova A. S., Chernin A. D., 1980, Afz, 16, 169

APPENDIX A1: THE TRAVELLING WAVELETS METHOD

The travelling wavelets method (Basdevant, Holschneider & Perrier 1990) applies to (non-linear) partial differential equations of the form

$$\frac{\partial f}{\partial t} + A_x f = 0.$$

It provides us with an approximate solution

$$f(x,t) = \sum_{i=1}^{N} \psi_i(x,t), \qquad \psi_i(x,t) = c_i \psi\left(\frac{x-b_i}{a_i}\right)$$

which reads as a finite sum of wavelets ψ_i called *atoms*. The function ψ is the *base wavelet*: it is defined upon a compact support and verifies $\int \psi(x)\mathrm{d}x = 0$. The time-dependent parameters a_i, b_i and c_i are respectively the scale, the position and the amplitude of the ith atom. The time derivatives of these parameters are obtained by minimizing the quantity

$$\int \left| \frac{\partial f}{\partial t} + A_x f \right|^2 \mathrm{d}x$$

at any time t. Hence, one obtains a linear system of ordinary differential equations in terms of $\dot{a}_i$, $\dot{b}_i$ and $\dot{c}_i$, which defines the resolution method.

Because of reasons of compactness, it turns out that two atoms i and j evolve independently provided the conditions

$$\left| \frac{a_j}{a_i} - 1 \right| \gg 0, \qquad \frac{|b_j - b_i|}{a_i} \gg 1$$

are fulfilled. Hence, one understands that the evolution of individual structures can be investigated separately, which is a major advantage compared with Fourier analysis. On the other hand, the differential system becomes numerically unstable when the above conditions are not satisfied, and the present mathematical framework does not account yet for such a situation. With this in mind, the solution space is reduced to a single atom, which limits the dynamics to be described solely by the evolution of the scale, the position and the amplitude of a wavelet. It must be noted that such a solution is less constrained than the linear regime, although being a simplified version of the dynamical behaviour of the gravitational instability.

APPENDIX A2: THE HERMITE FUNCTIONS

The aim of this section is to calculate the expression of J terms given in equation (29), which account for coupling effects between modes. Such calculations turn out to be easier to perform in Fourier space by using the integration by parts method. The first step is to calculate the Fourier transforms of base wavelets defined in equation (27). They are given as follows:

$$\hat{K}_n(k) = \frac{1}{\sqrt{2\pi}} \int K_n(x) \mathrm{e}^{\mathrm{i}kx} \mathrm{d}x = (\mathrm{i}k)^n \mathrm{e}^{-k^2/2}. \tag{A1}$$

The base wavelet $K(x)$ can be written by means of the following recurrence formula:

$$K_n(x) = xK_{n-1}(x) - (n-1)K_{n-2}(x), \tag{A2}$$

where $K_0(x) = \exp(-x^2/2)$ and $K_1(x) = xK_0(x)$, which can be obtained by calculating the inverse Fourier transforms:

$$\begin{aligned} K_n(x) &= \frac{1}{\sqrt{2\pi}} \int (\mathrm{i}k)^n \mathrm{e}^{-k^2/2} \mathrm{e}^{-\mathrm{i}kx} \mathrm{d}k \\ &= -\frac{\mathrm{i}}{\sqrt{2\pi}} \int (\mathrm{i}k)^{n-1} \mathrm{e}^{-\mathrm{i}kx} \mathrm{d}\left(\mathrm{e}^{-k^2/2}\right) \\ &= \frac{1}{\sqrt{2\pi}} \int \left[x(\mathrm{i}k)^{n-1} - (n-1)(\mathrm{i}k)^{n-2}\right] \mathrm{e}^{-\mathrm{i}kx - k^2/2} \mathrm{d}k. \end{aligned}$$

By using the recurrence formula given in equation (A2) down to the lowest order, the base wavelets transforms are

$$K_n(x) = 2^{-n/2} \mathrm{e}^{-x^2/2} H_n\left(\frac{x}{\sqrt{2}}\right) = \mathrm{e}^{-x^2/2} \sum_{i=0}^{n} h_i^n x^{\mathrm{i}}, \tag{A3}$$

where H_n is an Hermite polynomial, and the coefficients are given by

$$h_0^n = -(n-1)h_0^{n-2}, \tag{A4}$$

$$h_i^n = h_{i-1}^{n-1} - (n-1)h_i^{n-2}, \quad (1 \le i \le n-2), \tag{A5}$$

$$h_i^n = h_{i-1}^{n-1}, \quad (i = n-1, n), \tag{A6}$$

with $h_0^0 = 1$, $h_0^1 = 0$ and $h_1^1 = 1$; a little algebra gives

$$h_n^n = 1, \quad h_0^{2n} = (-1)^n \frac{(2n)!}{2^n n!}, \tag{A7}$$

if $i + n$ is odd then $h_i^n = 0$. (A8)

A2.1 Calculation of $J_{m;n}$

According to equation (29), we have

$$\begin{aligned} J_{m;n} &= a_1 \int \mathrm{d}y K_m(y) K_n(wy + v) \\ &= a_2 \int \mathrm{d}k_1 \hat{K}_m(k_1) \int \mathrm{d}k_2 \hat{K}_n\left(\frac{k_2}{w}\right) \mathrm{e}^{-\mathrm{i}k_2 v/w} \delta(k_1 + k_2) \\ &= (-1)^m \frac{a_2}{w^n} \int \mathrm{d}k_2 (\mathrm{i}k_2)^{m+n} \mathrm{e}^{-(1+w^{-2})k_2^2/2} \mathrm{e}^{-\mathrm{i}k_2 v/w} \\ &= (-1)^m \sqrt{2\pi} \frac{a_2}{w^n} \left(\frac{w}{\sqrt{1+w^2}}\right)^{m+n+1} \\ &\quad \times K_{m+n}\left(\frac{v}{\sqrt{1+w^2}}\right), \end{aligned}$$

where $y = y_1$, $w = a_1/a_2$ and $v = (b_1 - b_2)/a_2$; the second equality is obtained by writing the base wavelets as inverse Fourier transforms of their Fourier transforms; the integration over y gives the Dirac distribution function δ; using the integration over k_1, and according to equation A1, we obtain the third equality; by using the variable transform $k_2 \rightarrow k = k_2\sqrt{1+w^{-2}}$ and by recognizing the inverse Fourier transforms of $\hat{K}_{m+n}$, the integration over k gives the last equality. Finally, by substituting the original variables, we obtain

$$J_{m;n} = (-1)^m \mathcal{I}_{m;n} K_{m+n}\left(\frac{b_1 - b_2}{\sqrt{a_1^2 + a_2^2}}\right), \tag{A9}$$

where

$$\mathcal{I}_{m;n} = \sqrt{2\pi} \frac{a_1^{n+1} a_2^{m+1}}{\left(a_1^2 + a_2^2\right)^{(m+n+1)/2}}. \tag{A10}$$

Let us note that if $a_1 = a_2 = \alpha$ then

$$\mathcal{I}_{m;n} = \sqrt{\pi} 2^{-(m+n)/2} \alpha. \tag{A11}$$

Moreover, if $b_1 = b_2$ the J terms simplify with regard to the parity of integers m and n, one has

$$J_{m;n} = \begin{cases} 0 & \text{if } m + n = 2p + 1, \\ (-1)^{(n-m)/2} (2p)!/2^p p! \mathcal{I}_{m;n} & \text{if } m + n = 2p, \end{cases} \tag{A12}$$

equations (A7) and (A8).

A2.2 Calculation of $J_{m,n;p}$

According to equation (29), we have

$$\begin{aligned} J_{m,n;p} &= a_1 \int \mathrm{d}y K_m(y) K_n(y) K_p(wy + v) \\ &= \frac{a_2}{\sqrt{2\pi}} \int \mathrm{d}k_1 \hat{K}_m(k_1) \int \mathrm{d}k_2 \hat{K}_n(k_2) \\ &\quad \times \int \mathrm{d}k_3 \hat{K}_p\left(\frac{k_3}{w}\right) \mathrm{e}^{-\mathrm{i}k_3 v/w} \delta(k_1 + k_2 + k_3) \\ &= \frac{a_2}{\sqrt{2\pi}} \int \mathrm{d}k_1 \hat{K}_m(k_1) \int \mathrm{d}k_2 \hat{K}_n(k_2) \\ &\quad \times \frac{(-1)^p}{w^p} \hat{K}_p(k_1 + k_2) \mathrm{e}^{\mathrm{i}(k_1+k_2)v/w} \\ &= \frac{a_2}{\sqrt{2\pi}} \frac{(-1)^p}{w^p} \sum_{j=0}^{p} \frac{p!}{j!(p-j)!} \\ &\quad \times \int \mathrm{d}k_1 \left(\mathrm{i}k_1\right)^{m+j} \mathrm{e}^{-k_1^2(1+w^{-2})} \mathrm{e}^{\mathrm{i}k_1 v/w} \\ &\quad \times \int \mathrm{d}k_2 \left(\mathrm{i}k_2\right)^{n+p-j} \mathrm{e}^{-k_2^2(1+w^{-2})} \mathrm{e}^{\mathrm{i}k_2 v/w} \mathrm{e}^{-k_1 k_2} \\ &= \frac{a_2}{\sqrt{2\pi}} \frac{(-1)^p w^{m+n+2}}{(1+w^2)^{(m+n+p+2)/2}} \sum_{l\geq 0} \frac{1}{l!} \left(\frac{w^2}{1+w^2}\right)^l \\ &\quad \times \sum_{j=0}^{p} \frac{p!}{j!(p-j)!} \int \mathrm{d}k_1 \hat{K}_{m+j+l}(k_1) \mathrm{e}^{(\mathrm{i}k_1 v/\sqrt{1+w^2}} \\ &\quad \times \int \mathrm{d}k_2 \hat{K}_{n+p-j+l}(k_2) \mathrm{e}^{(\mathrm{i}k_2 v)/\sqrt{1+w^2}} \\ &= a_2 \sqrt{2\pi} \frac{(-1)^{m+n} w^{(m+n+2}}{(1+w^2)^{(m+n+p+2)/2}} \\ &\quad \times \sum_{l\geq 0} \frac{1}{l!} \left(\frac{w^2}{1+w^2}\right)^l \sum_{j=0}^{p} \frac{p!}{j!(p-j)!} \\ &\quad \times K_{m+j+l}\left(\frac{v}{\sqrt{1+w^2}}\right) K_{n+p-j+l}\left(\frac{v}{\sqrt{1+w^2}}\right), \end{aligned}$$

where the notations are given above and the integration technique is similar; the first two equalities are trivial and the third one is obtained from the integration over k_3, the following one by writing the expression of $\hat{K}$ functions and by expanding the term $(\mathrm{i}k_1 + \mathrm{i}k_2)^p$; by using the variable transform $k_2 \rightarrow k = k_2\sqrt{1+w^{-2}}$ and writing the correlation term $\mathrm{e}^{-k_1 k_2}$ as an exponential expansion the two integrals decouple, and we obtain the fifth equality; and by recognizing the inverse Fourier transforms, we obtain the last equality. Finally, by substituting the original variables, we obtain

$$\begin{aligned} J_{m,n;p} &= (-1)^{m+n} \mathcal{I}_{m,n;p} \sum_{l\geq 0} \frac{1}{l!} \left(\frac{a_1^2}{a_1^2 + a_2^2}\right)^l \\ &\quad \times \sum_{j=0}^{p} \frac{p!}{j!(p-j)!} K_{m+j+l}\left(\frac{b_1 - b_2}{\sqrt{a_1^2 + a_2^2}}\right) \\ &\quad \times K_{n+p-j+l}\left(\frac{b_1 - b_2}{\sqrt{a_1^2 + a_2^2}}\right), \end{aligned} \tag{A13}$$

where

$$\mathcal{I}_{m,n;p} = \sqrt{2\pi} \frac{a_1^{m+n+2} a_2^{p+1}}{(a_1^2 + a_2^2)^{(m+n+p+2)/2}}. \tag{A14}$$

Note that if $a_1 = a_2 = \alpha$ then one has

$$\mathcal{I}_{m,n;p} = \sqrt{\frac{\pi}{2}} 2^{-(m+n+p)/2} \alpha. \tag{A15}$$

As in Section A2.1, if $b_1 = b_2$ then the J terms accounts for the parity properties of integers m, n and p. Indeed, note that the only way to have $K_{m+j+l}(0) K_{n+p-j+l}(0) \neq 0$ is that both $m + j + l$ and $n + p - j + l$ must be even integers, which implies that $m + n + p$ is even as well.

APPENDIX A3: THE FUNCTION τ

Let us show that the function $\tau_0(m, n)$ given in equation (43) satisfies the inequality

$$0 < \tau_0(m, n) \leq 1. \tag{A16}$$

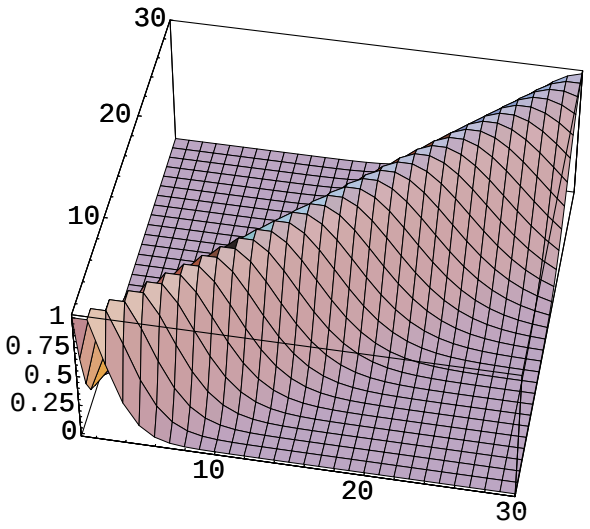

Figure A1. 3D plot of the function $\tau_0(2m, 2n)$.

It is clear that if $n - m = 0, 2$ then $\tau_0 = 1$, otherwise one has two cases, which are either $m > n$ or $m < n - 2$.

(i) If $(m > n)$ then we can write $m = n + 2i$ with $i \geq 1$, and the function τ_0 reads

$$\tau_0(n + 2i, n) = \frac{(2n + 2i + 1)!!(2n + 2i - 1)!!}{(2n + 4i + 1)!!(2n - 1)!!}.$$

Hence, we use a recurrence upon i, by assuming that the inequality is valid for any $j \leq i$: one has (for $i + 1$)

$$\tau_0(n + 2i + 2, n) = \frac{(2n + 2i + 3)!!(2n + 2i + 1)!!}{(2n + 4i + 5)!!(2n - 1)!!}$$
$$= \frac{(2n + 2i + 3)(2n + 2i + 1)}{(2n + 4i + 5)(2n + 4i + 3)} \tau_0(n + 2i, n)$$
$$< \frac{(2n + 2i + 3)(2n + 2i + 1)}{(2n + 4i + 5)(2n + 4i + 3)}$$
$$< 1.$$

(ii) If $(m < n - 2)$ then we can write $n = m + 2i$ with $i \geq 2$, and the function τ_0 reads

$$\tau_0(m, m + 2i) = \frac{(2m + 2i + 1)!!(2m + 2i - 1)!!}{(2m + 1)!!(2m + 4i - 1)!!},$$

Using a similar reasoning to that above, one has (for $i \neq 0$)

$$\tau_0(m, m + 2i + 2) = \frac{(2m + 2j + 3)!!(2m + 2i + 1)!!}{(2m + 1)!!(2m + 4i + 3)!!}$$
$$< \frac{(2m + 2i + 3)(2m + 2i + 1)}{(2m + 4i + 3)(2m + 4i + 1)}$$
$$< 1.$$

Therefore, we see that the function $\tau_0(2m, 2n)$ is a decreasing function of $|m - n|$ (see Fig. A1). The same holds true for the function $\tau_0(2m + 1, 2n + 1)$.

APPENDIX A4: LAGRANGIAN INTERPRETATION

The aim of this section is to compare our results to Zentsova & Chernin's (1980) solution (hereafter ZC), which has been derived from a Lagrangian scheme. In general, the translation of a Lagrangian scheme into an Eulerian one, and vice versa, is quite a difficult task from a mathematical point of view. A helpful reference for the inversion of Lagrangian models is Susperregi & Buchert (1997). Although the interpretation can be reduced into a more simple formalism for a 1D system some difficulties still remain because of implicit definitions of functions. Nevertheless, a Lagrangian interpretation of wavelet profiles can be obtained under some hypothesis, and a rough comparison of wavelets behaviour to the ZC solution can also be performed.

A4.1 Eulerian/Lagrangian formalism

Let us assume a pressureless system of sources moving within a Friedmann cosmological background (used as 'body'). The displacement of a test particle which lies at initial comoving coordinate q_1 at time $t = t_0$ can be written as

$$t \mapsto x = q_1 + F(q_1, t). \tag{A17}$$

The function

$$q_1 \mapsto F(q_1, t), \qquad F(q_1, t_0) = 0, \tag{A18}$$

defines the Lagrangian scheme. The Eulerian interpretation is given by *implicit* definitions of the density contrast and the scaled peculiar velocity fields, as follows:

$$\delta(x, t) = \left[1 + \delta_0(q_1)\right] \left[1 + \frac{\partial F}{\partial q_1}(q_1, t)\right]^{-1} - 1, \tag{A19}$$

$$u(x, t) = \frac{\partial F}{\partial t}(q_1, t), \tag{A20}$$

where $\delta_0(q_1) = \delta(q_1, t_0)$ stands for the initial density profile, and the argument x is given by equation (A17). Such a definition enables us to investigate the evolution with time of individual structures. On the other hand, it does not provide us with a pure Eulerian description in term of fields at a given constant coordinate x. It is also important to mention some limitations of such an approach. Indeed, equation (A19) is obtained from the equality

$$\delta_0(q_1) \mathrm{d}q_1 = \rho(x, t) \mathrm{d}x, \tag{A21}$$

which accounts for the conservation of the trajectory flow. However, such a property is valid as long as the mapping $q_1 \mapsto x$ stands for a coordinate transform, which means that the condition

$$\frac{\partial F}{\partial q_1} \neq -1 \tag{A22}$$

must be fulfilled within the q_1 value domain. It is clear that, if a one-to-one mapping is required only between the initial and final positions, then this model must account for particular physical conditions of the medium which make the test particles ignore each other. On the other hand, with respect to a physical viewpoint, it is also clear that equation (A22) must be fulfilled from t_0 up to t, in order to avoid trajectory crossing problems. The validity of this model is discussed in detail by Zel'dovich (1970a, b) and Shandarin & Zel'dovich (1984, 1989), see also Doroshkevich & Shandarin (1973) and Doroshkevich et al. (1973).

On the way around, the determination of the function $F(q_1, t)$ from equation (A19, A20) demands to invert equation (A17). This is an implicit problem to solve. The translation of an Eulerian scheme into a Lagrangian formalism is made easier by using the function

$$t \mapsto q_1 = x - \tilde{F}(x, t), \qquad \tilde{F}(x, t_0) = 0, \tag{A23}$$

which is a solution of the equation

$$\frac{\mathrm{d}\tilde{F}}{\mathrm{d}t}(x, t) = u(x, t). \tag{A24}$$

This function gives the initial Lagrangian coordinates $q_1 = q_1(x, t)$

at time $t = t_0$ of the test particle that lies at coordinate x at time t. A similar reasoning to the one above provides us with the following *implicit* equation system:

$$\frac{\partial \tilde{F}}{\partial x}(x,t) = \frac{\delta_0(q_1) - \delta(x,t)}{1+\delta_0(q_1)}, \tag{A25}$$

$$\frac{\partial \tilde{F}}{\partial t}(x,t) = \frac{1+\delta(x,t)}{1+\delta_0(q_1)}\, u(x,t) \tag{A26}$$

where q_1 is given by equation (A23), from which the displacement $F(q_1,t) = \tilde{F}(x,t)$ can be estimated, by substituting the Eulerian fields $\delta(x,t)$ and $u(x,t)$ according to equations (13)–(15) by their Gaussian type shapes.

According to above descriptions, we easily understand that because the Lagrangian/Eulerian translations of the dynamics are not defined explicitly (but by implicit formulas), the interpretation of the evolution of structures in term of travelling wavelet characteristics is not as simple as that. However, under the hypothesis

$$\delta_0(q_1) \approx 0, \tag{A27}$$

which means that the structure formation is induced from the background mainly by velocity gradients, one has a quite straightforward interpretation. Indeed, according to equation (A25) one has

$$\frac{\partial \tilde{F}}{\partial x}(x,t) \approx -\delta(x,t). \tag{A28}$$

This equality, with equation (15), provides us with the interpretation of Lagrangian displacements in term of travelling wavelets as follows:

$$\tilde{F}(x,t) \approx -c_2 \hat{\psi}_2\left(\frac{x-b_2}{a_2}\right), \tag{A29}$$

up to a time-dependent function. It is interesting to note that if the same wavelet is used for the density contrast and the velocity fields ($\hat{\psi}_1 = \hat{\psi}_2$), and the scale and position parameters are kept identical and constant ($a_1 = a_2 = \alpha$ and $b_1 = b_2 = \beta$), then such a displacement can be written as a product of a time-dependent function times a space-dependent function. Although these are typical features of the linear regime, we know that parity properties for the modes are also required, according to Section 4.1. These features interpret Zel'dovich's (1970a) approach in term of wavelet criteria, which extrapolate the linear theory of gravitational instability into the nonlinear regime.

A4.2 The Zentsova & Chernin solution

In this section in addition to deriving the ZC solution, we shed enlightenment on the 1D ansatz defined by equations (2)–(4). The ZC solution is obtained by interpreting the constraints related to 3D Euler–Poisson equations on the displacement function given by Eq. (68). Hence, one obtains a differential equation which can be easily integrated.

For a 1D flow (the velocity of particles is parallel to their acceleration), the 3D position of a test particle which lies at initial coordinate $\boldsymbol{q}$ at time $t = t_0$ reads

$$t \mapsto \boldsymbol{r} = a\boldsymbol{q} + \epsilon(q_1,t)\boldsymbol{\eta}, \quad \boldsymbol{\eta} = \begin{pmatrix} 1 \\ 0 \\ 0 \end{pmatrix}, \tag{A30}$$

where $a = a(t)$ is the dimensionless expansion parameter and

$$q \mapsto \epsilon(q_1,t) = a(t)F(q_1,t), \qquad \epsilon(q_1,t_0) = 0, \tag{A31}$$

where F is the displacement function defined in equation (A18), and its velocity is given by

$$t \mapsto \boldsymbol{v} = \frac{\partial \boldsymbol{r}}{\partial t} = \dot{a}\boldsymbol{q} + \frac{\partial \epsilon}{\partial t}\boldsymbol{\eta}. \tag{A32}$$

The 3D Euler–Poisson equations read

$$\frac{\mathrm{d}\boldsymbol{v}}{\mathrm{d}t} = -\nabla_r \varphi \tag{A33}$$

$$\frac{\mathrm{d}\rho}{\mathrm{d}t} = -\rho \nabla_r \cdot \boldsymbol{v} \tag{A34}$$

$$\Delta\varphi = 4\pi\rho, \tag{A35}$$

where ∇_r stands for the gradient operator with respect to r coordinates, and one has

$$\frac{\partial}{\partial r_1} = \left(a + \frac{\partial \epsilon}{\partial q_1}\right)^{-1} \frac{\partial}{\partial q_1}, \quad \frac{\partial}{\partial r_{i=2,3}} = a^{-1}\frac{\partial}{\partial q_i}. \tag{A36}$$

The projection of these equations on to the comoving space provides us with the 1D ansatz defined by equations (2)–(4), where $x = a^{-1}r_1$ and $u = a^{-1}\partial\epsilon/\partial t$, as long as the 3D flow is described by equation (A30).

According to equations (A33) and (A35), one has

$$-4\pi\rho = \nabla_r \cdot \left(\frac{\mathrm{d}\boldsymbol{v}}{\mathrm{d}t}\right) \tag{A37}$$

$$= \left(\ddot{a} + \frac{\partial}{\partial q_1}\frac{\partial^2 \epsilon}{\partial t^2}\right)\left(a + \frac{\partial \epsilon}{\partial q_1}\right)^{-1} + 2\frac{\ddot{a}}{a} \tag{A38}$$

according to equations (A32) and (A36). Hence, the constraint on the 3D displacement is given by the following differential equation:

$$3\ddot{a} + \kappa = -4\pi\rho\left(a + \frac{\partial \epsilon}{\partial q_1}\right), \tag{A39}$$

where the function

$$\kappa(q_1,t) = \left(\frac{\partial^2}{\partial t^2} + 2\frac{\ddot{a}}{a}\right)\frac{\partial \epsilon}{\partial q_1}, \quad \kappa(q_1,t_0) = 0. \tag{A40}$$

Let us emphasize that this function has a vanishing value at $t = t_0$ because $\epsilon(q_1,t_0) = 0$ for all q_1, see equation (A31).

According to equations (A32) and (A36), equation (A34) transforms to

$$\frac{\mathrm{d}\rho}{\rho} = -\left(\nabla_r \cdot \boldsymbol{v}\right)\mathrm{d}t = -2\frac{\dot{a}}{a}\mathrm{d}t - \left(a + \frac{\partial \epsilon}{\partial q_1}\right)^{-1}\left(\dot{a} + \frac{\partial}{\partial q_1}\frac{\partial \epsilon}{\partial t}\right)\mathrm{d}t \tag{A41}$$

which integrates easily by identifying the terms with derivatives of logarithm functions, and thus provides us with the energy density field

$$\rho(\boldsymbol{r},t) = \rho(\boldsymbol{q},t_0)\left(\frac{a}{a_0}\right)^{-3}\left[1 + \frac{1}{a}\frac{\partial \epsilon}{\partial q_1}(q_1,t)\right]^{-1}, \tag{A42}$$

in terms of initial conditions. Therefore, according to equations (A39) and (A42), the ratio

$$\frac{3\ddot{a} + \kappa(q_1,t)}{3\ddot{a}_0 + \kappa(q_1,t_0)} = \left(\frac{a}{a_0}\right)^{-2} \tag{A43}$$

shows that

$$3\ddot{a}a^2 + \kappa(q_1,t)a^2 = 3\ddot{a}_0 a_0^2 \tag{A44}$$

is a constant term, see equation (A40). The evolution of the expansion parameter is governed by Friedmann equations,

$$\ddot{a}a^2 = \frac{1}{3}\left(\Lambda a^3 - 4\pi\bar{\rho}_0\right), \tag{A45}$$

$$\left(\frac{\dot{a}}{a}\right)^2+\frac{k}{a^2}=\frac{8}{3}\pi\bar{\rho}_0 a^{-3}+\frac{\Lambda}{3}, \tag{A46}$$

which provide us with two constant terms

$$\alpha_1=\ddot{a}a^2-\frac{\Lambda}{3}a^3=\ddot{a}_0a_0^2-\frac{\Lambda}{3}a_0^3, \tag{A47}$$

$$\alpha_2=\dot{a}^2a+ka-\frac{\Lambda}{3}=\dot{a}_0^2a_0+ka_0-\frac{\Lambda}{3}. \tag{A48}$$

Hence, equation (A44) transforms to

$$\left[\left(\frac{\alpha_2}{a}-k+\frac{\Lambda}{3}a^2\right)\frac{\partial^2}{\partial a^2}+\left(\frac{\alpha_1}{a^2}+\frac{\Lambda}{3}a\right)\frac{\partial}{\partial a}+2\left(\frac{\alpha_1}{a^3}+\frac{\Lambda}{3}\right)\right]\frac{\partial\epsilon}{\partial q_1}=\Lambda\left(\frac{a_0^3}{a^2}-a\right), \tag{A49}$$

and for a flat space ($k=0$) and a vanishing cosmological constant ($\Lambda=0$), equation (A49) transforms to

$$\left(a^2\frac{\partial^2}{\partial a^2}-\frac{a}{2}\frac{\partial}{\partial a}-1\right)\frac{\partial\epsilon}{\partial q_1}=0. \tag{A50}$$

The solution is the polynomial

$$\frac{\partial\epsilon}{\partial q_1}=C_1(q_1)\left(\frac{a}{a_0}\right)^2-C_2(q_1)\left(\frac{a}{a_0}\right)^{-1/2}, \tag{A51}$$

where we have, necessarily,

$$C(q_1)=C_1(q_1)=C_2(q_1), \tag{A52}$$

which stands for the only[5] arbitrary function of q_1. Hence, we have

$$\frac{\partial F}{\partial q_1}=\frac{1}{a}\frac{\partial\epsilon}{\partial q_1}=\frac{C(q_1)}{a_0}\left[\left(\frac{a}{a_0}\right)-\left(\frac{a}{a_0}\right)^{-3/2}\right] \tag{A53}$$

with $a/a_0=\left[1+3/2\times H_0(t-t_0)\right]^{2/3}\propto t^{2/3}$, which has to be substituted in equation (A19). Hence, the displacement function $F(q_1,t)$ can be determined to be an additive time-dependent function which must be vanishing at $t=t_0$. However, such a function is not taken into account because it stands for global displacement. Therefore, by referencing with respect to a particle which follows the Hubble expansion, one can write

$$F(q_1,t)=\frac{\hat{C}(q_1)}{a_0}\left[\left(\frac{a}{a_0}\right)-\left(\frac{a}{a_0}\right)^{-3/2}\right], \tag{A54}$$

where $C=\mathrm{d}\hat{C}/\mathrm{d}q_1$.

Finally, according to equations (A53), (A19) and (A20), we can see that the Eulerian field defined by the ZC solution is fully defined by initial conditions upon the functions $\delta_0(q_1)$ and $\hat{C}(q_1)$.

The most straightforward method to test our results is to use the following equations:

$$\frac{1+\delta_0(q_1)}{1+\delta(x,t)}=1+\frac{C(q_1)}{a_0}\left[\left(\frac{a}{a_0}\right)-\left(\frac{a}{a_0}\right)^{-3/2}\right] \tag{A55}$$

$$u(x,t)=\frac{\hat{C}(q_1)}{a_0}\frac{\dot{a}}{a}\left[\left(\frac{a}{a_0}\right)+\frac{3}{2}\left(\frac{a}{a_0}\right)^{-3/2}\right], \tag{A56}$$

with $a/a_0\propto t^{2/3}$ and $\dot{a}/a\propto t^{-1}$, where the Eulerian fields are substituted by their wavelet profiles with x given by equation (A17). Hence, we understand that a formal comparison of the ZC solution to wavelet behaviour cannot be carried out simply.

This paper has been typeset from a TEX/LATEX file prepared by the author.

[5] It must be emphasized that the ZC solution does not impose such a constraint when the equality $\epsilon(q_1,t_\circ)=0$ must be verified for all q_1.